# Stimulated emission mechanism of aluminum nitride

Ryota Ishii [1,*] Toru Nagashima,[2] Reo Yamamoto,[2] Tatsuya Hitomi,[2] Mitsuru Funato [1] and Yoichi Kawakami [1]
[1] *Department of Electronic Science and Engineering, Kyoto University, Kyoto 615-8510, Japan*
[2] *Tsukuba Research Laboratories, Tokuyama Corporation, Tsukuba, Ibaraki 300-4247, Japan*

(Received 7 January 2022; revised 9 May 2022; accepted 11 May 2022; published 27 May 2022)

Photoluminescence and stimulated emission spectroscopies were performed on transparent aluminum nitride (AlN) substrates grown by hydride vapor-phase epitaxy. The stimulated emission was observed from cryogenic to room temperatures and its origin was assigned on the basis of the spontaneous emission spectra and existing theories. Two stimulated emission mechanism crossovers were also found. One was a temperature-induced crossover from a purely excitonic mechanism to a carrier-involved mechanism, which is a universal behavior in semiconducting materials. The other was an excitation-power–induced crossover from an exciton–exciton scattering mechanism to a phonon-mediated mechanism, which is a unique behavior attributed to the peculiar excitonic structure (negative crystal-field splitting and positive electron–hole exchange interaction energies) of AlN.

DOI: 10.1103/PhysRevB.105.205206

## I. INTRODUCTION

Aluminum nitride (AlN) and its related compounds have attracted much attention as deep-ultraviolet (DUV) -emitting materials [1–3]. Recent studies have demonstrated DUV-emitting laser diodes (LDs) based on aluminum gallium nitride (AlGaN) active layers [4,5]. However, AlGaN-based LDs currently have a shortcoming in that the laser operation is limited under pulsed conditions with a relatively high threshold current density (>10 kA/cm$^2$), indicating that the physics of stimulated emission in AlGaN should be further examined. Previous studies have mainly focused on the device physics of AlGaN-based LDs to reduce the threshold power/current density [6–10], whereas the stimulated emission mechanism (e.g., from excitonic or electron–hole plasma states) has received less attention despite the importance noted in early II–VI semiconductor research [11–19]. Excitons play a more important role in AlN because of its larger exciton binding energy compared with that in II–VI semiconductors [20]. Murotani *et al.* have investigated the gain generation mechanism of AlGaN quantum wells [21]. However, their sample showed broad spontaneous and stimulated emission spectra because of its alloy composition and/or quantum-well width disorder, which prevented an unambiguous resolution of the stimulated emission mechanism of AlGaN. Studying the stimulated emission mechanisms of binary constituents is an alternative approach to elucidate the stimulated emission mechanisms of ternary semiconductors. The stimulated emission mechanism of gallium nitride (GaN) has been a subject of numerous investigations [22–26], whereas that of AlN has yet to be studied. Only one report just observed stimulated emission at room temperature from AlN layers epitaxially overgrown laterally on sapphire substrates [27]. Therefore, we herein spectroscopically investigate the stimulated emission mechanism of AlN from cryogenic to room temperatures to satisfy both scientific interests and industrial requirements. We observe excitation-power- and temperature-induced crossover of the stimulated emission mechanism and assign the origin of the stimulated emission lines on the basis of the spontaneous emission spectra and existing theories.

## II. EXPERIMENTAL METHODS

We investigated transparent *c*-plane AlN single crystals grown by the hydride vapor-phase epitaxy (HVPE) method [28,29]. The sample was 327 $\mu$m thick. The x-ray rocking curves of the (0002) symmetric and $(10\bar{1}1)$ asymmetric planes were 13 arcsec and 11 arcsec (close to the detection limit), respectively. The total threading dislocation density was estimated using the etch-pit method to be less than $5 \times 10^4$ cm$^{-2}$. The *a*-axis and *c*-axis lattice constants were 3.1110 Å ($3\sigma = 0.00022$ Å) and 4.9812 Å ($3\sigma = 0.00002$ Å), respectively. The boron, carbon, oxygen, silicon, and chlorine concentrations were $2.6 \times 10^{15}$ cm$^{-3}$, $4.8 \times 10^{15}$ cm$^{-3}$ (near the detection limit), $3.6 \times 10^{17}$ cm$^{-3}$, $9.8 \times 10^{16}$ cm$^{-3}$, and $1.7 \times 10^{14}$ cm$^{-3}$, respectively. Unlike physical-vapor-transport-grown AlN substrates, our sample was transparent in both the visible [Fig. 1(a)] and ultraviolet [Fig. 1(b)] spectral regions.

Temperature-dependent photoluminescence (PL) and stimulated emission spectroscopies were performed using a pulsed ArF excimer laser (ATLEX S 300, ATL Lasertechnik GmbH). The far-field beam pattern was a rectangular shape. The excitation wavelength and pulse duration were ∼193 nm and ∼6.5 ns, respectively. The repetition rate was set at 50 Hz and 10 Hz for PL and stimulated emission measurements, respectively. Luminescence signals were dispersed by a 50-cm monochromator (SP2500, Princeton Instruments) and detected by a liquid-$N_2$-cooled charge-coupled device (SPEC-10, Princeton Instruments). The spectral resolution was better than 3 meV. For PL measurements, samples were

*ryota.ishii@optomater.kuee.kyoto-u.ac.jp

 ©2022 American Physical Society

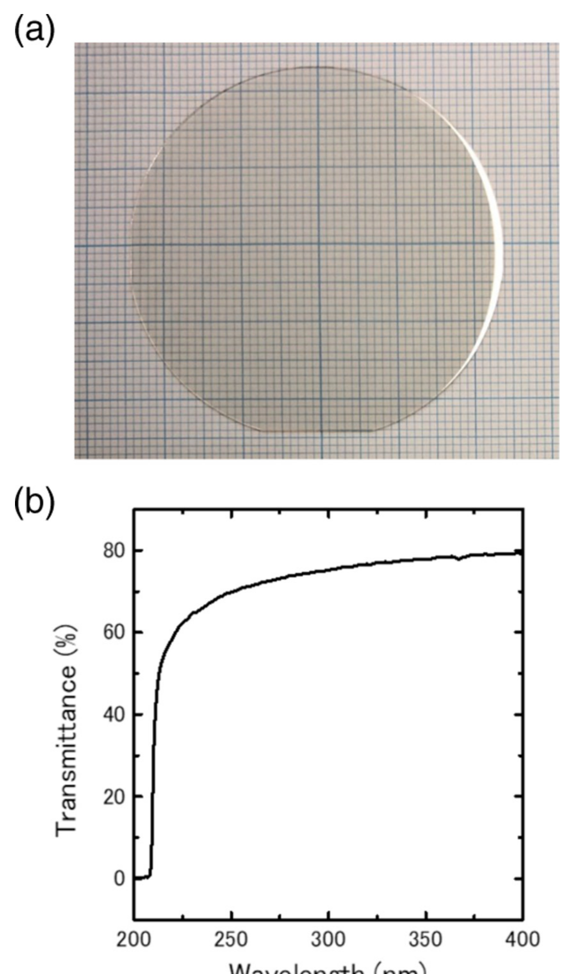


FIG. 1. (a) Photograph of a HVPE-grown AlN substrate with a diameter of 48 mm. (b) Ultraviolet transmittance spectrum of the sample at room temperature.

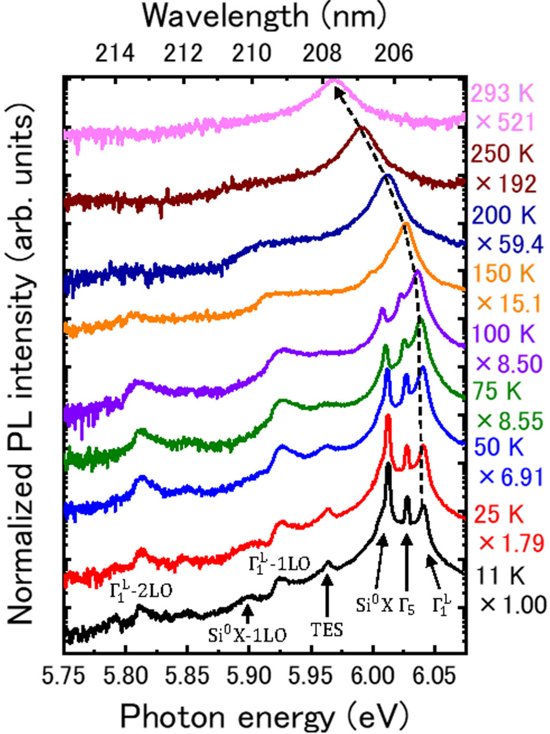


FIG. 2. Temperature-dependent PL spectra of a HVPE-grown AlN substrate. The PL spectra are vertically shifted for clarity. The factor used to normalize each PL spectrum is also given. The excitation power density is approximately 180 kW/cm$^2$.

excited from the surface normal through a spherical lens and the luminescence signals were detected at an angle of 60° from the surface normal. For stimulated emission measurements, samples were excited from the surface normal through a cylindrical lens. The sample was cleaved at the *m* plane and was 2.5 mm long. The luminescence signals were detected from the *m* plane (under edge-emission geometry). A closed-cycle conduction-cooling cryostat was used to control the experimental temperatures.

## III. EXPERIMENTAL RESULTS

Figure 2 shows temperature-dependent PL spectra of the HVPE-grown AlN substrate. The origins of the emission peaks at 11 K are assigned as follows. The 6.041 eV and 6.027 eV peaks are assigned to the radiative recombination of a free exciton, with irreducible representations of $\Gamma_1^L$ and $\Gamma_5$, respectively [30–35]. Note that the superscript in the former indicates longitudinal-wave character [35]. Although difficult to observe in Fig. 2 (see Fig. S4 in the Supplemental Material [36]), the peak at 6.032 eV is assigned to a free excitonic transverse-wave state with an irreducible representation of $\Gamma_1^T$ [35]. The 6.012 eV peak is assigned to the radiative recombination of the neutral Si-donor–bound exciton ($Si^0X$) [37,38]. The 5.964 eV peak is assigned to the two-electron satellite (TES) transition of a neutral Si-donor–bound exciton [38,39]. Because the longitudinal-optical (LO) phonon energy of AlN is ∼111 meV at cryogenic temperatures [40], the peaks at 5.924 eV and 5.90 eV are assigned to free ($\Gamma_1^L$-1LO) and bound ($Si^0X$-1LO) exciton transitions involving one LO phonon emission, respectively [41]. Similarly, the peak at 5.81 eV is assigned to a free exciton transition with two LO phonon emissions ($\Gamma_1^L$-2LO). It should be noted that the absolute PL peak energies differ slightly from those in previous studies [31,33–35,37–39,41] because of the difference in the residual strain among the freestanding AlN specimens. The strain-induced effect has been detailed elsewhere [42,43]. The temperature-dependent energy shift of the $\Gamma_1^L$ emission is clearly observed from cryogenic to room temperatures. The assignment of these spontaneous emission lines provides a guide for interpreting the following stimulated emission lines of AlN.

Figure 3 shows excitation-power–dependent luminescence spectra of the HVPE-grown AlN substrate, as recorded under the edge-emission geometry. At 11 K [Fig. 3(a)], the peak at 5.960 eV (denoted as $P^\infty$) first increases superlinearly (hereafter, it is denoted as first threshold.); the peak at 5.927 eV (denoted as $\Gamma_1^T$-1LO) then overtakes the $P^\infty$ band as the excitation power increases (hereafter, it is denoted as second threshold.). Figure 4 shows excitation-power-density dependence of the integrated emission intensity and the full width at half maximum (FWHM) of the main emission peak

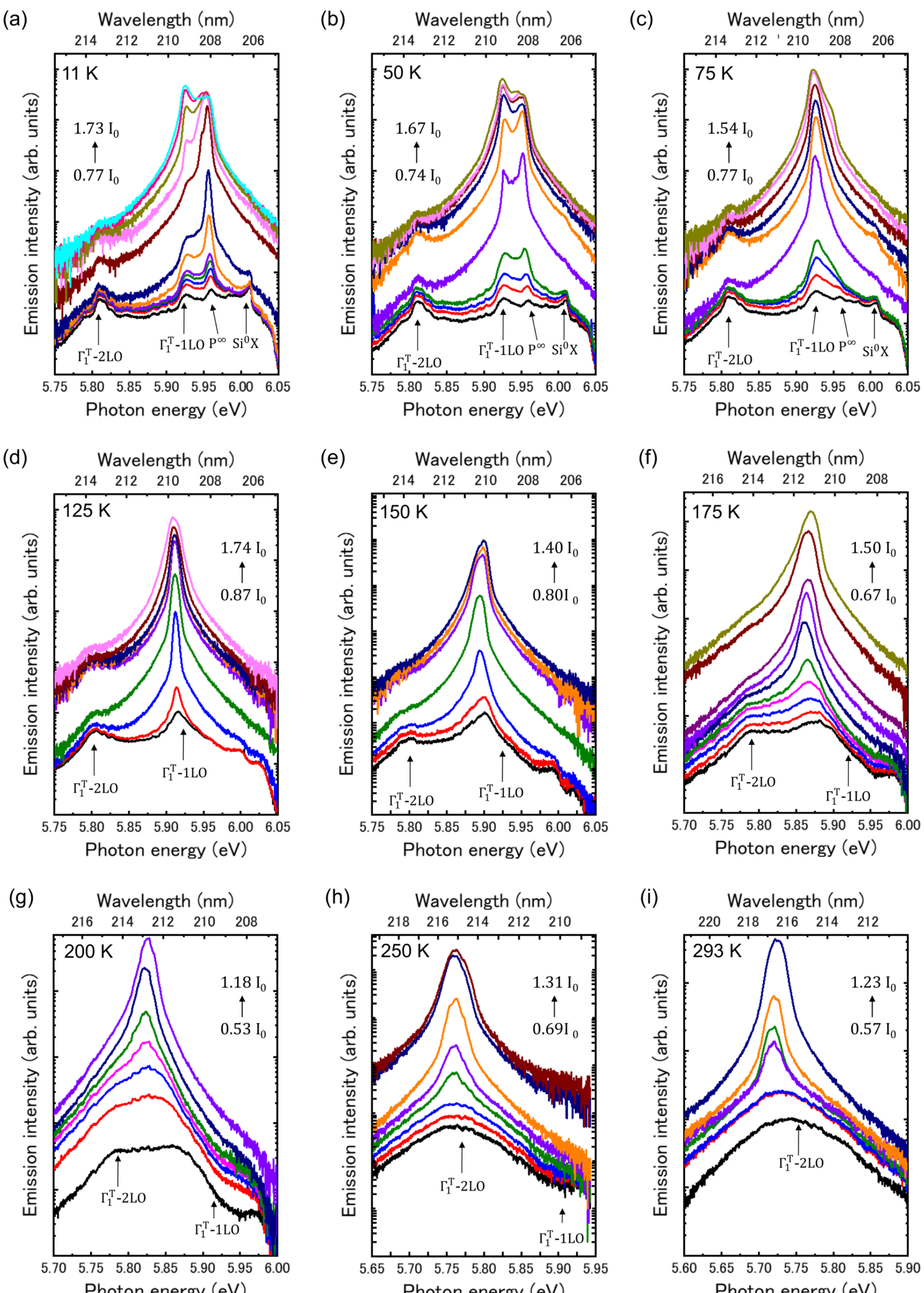


FIG. 3. Excitation-power–dependent luminescence spectra of a HVPE-grown AlN substrate, as recorded under an edge-emission geometry, at (a) 11 K, (b) 50 K, (c) 75 K, (d) 125 K, (e) 150 K, (f) 175 K, (g) 200 K, (h) 250 K, and (i) 293 K. The change in excitation-power density is written in the figures, where $I_0$ is the threshold power density shown in Fig. 6. The increment of the excitation-power density can be found from Fig. S6 in the Supplemental Material [36]. The peak energy position of the $\Gamma_1^T$-$m$LO spontaneous emissions is derived from Eq. (1).

at 11 K. Stimulated emission from semiconductors is usually identified by the occurrence of one or several of the following criteria: a superlinear increase of an optical output, a simultaneous spectral narrowing of an emission (often accompanied by an appearance of longitudinal laser modes), a spatially directed emission, and an increase of the coherence length of an emission above a threshold [44]. We judge the occurrence of stimulated emission in AlN from two of the above criteria: the superlinear increase of the optical output and the accompanying spectral narrowing of the emission shown in Fig. 4 (the quantitative details at other temperatures are described in the Supplemental Material [36]). Because the cavity

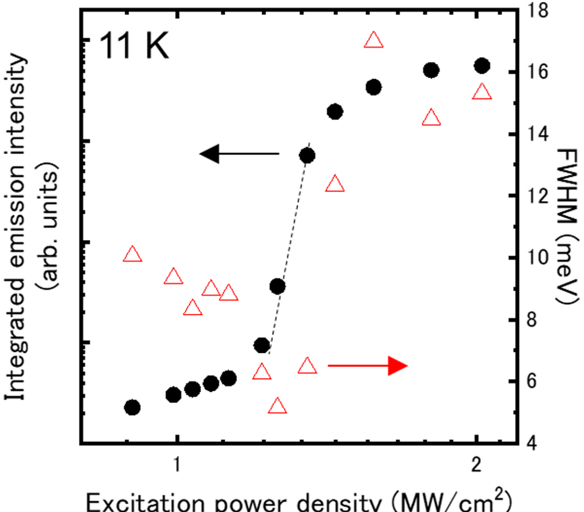


FIG. 4. Excitation-power-density dependence of the integrated emission intensity of the emission spectra (black solid circles) and the full width at half maximum (FWHM) of the main emission peak (red open triangles) for a HVPE-grown AlN substrate, as recorded under an edge-emission geometry at 11 K.

length of our sample is relatively long (2.5 mm), we cannot resolve the longitudinal laser modes due to the limited spectral resolution of our experimental setup. The excitation-power dependence of the luminescence spectra is approximately the same from 11 K to 50 K [Figs. 3(a)–3(b)]. At 75 K [Fig. 3(c)] and 100 K, the $\Gamma_1^{\mathrm{T}}$-1LO band exhibits stimulated emission behavior and is consistently the most dominant emission. At 125 K [Fig. 3(d)], the $\Gamma_1^{\mathrm{T}}$-1LO band likely shows stimulated emission, as evidenced by the high-energy tail spectral shape [45,46], although the stimulated emission peak is slightly redshifted from the spontaneous emission peak of the $\Gamma_1^{\mathrm{T}}$-1LO band. From 150 K to 200 K [Figs. 3(e)–3(g)], the stimulated emission peak energies do not coincide with any of the spontaneous emission peak energies in Fig. 2. From 225 K to 293 K [Figs. 3(h)–3(i)], the stimulated emission appears near the $\Gamma_1^{\mathrm{T}}$-2LO spontaneous emission peak energies. The similar spectral feature from 250 K to 293 K suggests the same origin of the stimulated emission. At 293 K, the stimulated emission exhibits a peak energy of 5.72 eV. By comparison, Shatalov *et al.* have reported room-temperature (RT) stimulated emission from heteroepitaxial AlN layers at 214.5 nm (5.79 eV) [27]. The high-energy shift of the heteroepitaxial AlN layers likely originates from the biaxial compressive strain generated by heteroepitaxy [32,43].

## IV. DISCUSSION

Below, we discuss the stimulated emission mechanism of AlN in terms of free-exciton LO-phonon replica (EX-$m$LO band), exciton–exciton scattering (P band), exciton–electron scattering (H band), and electron–hole plasma (EHP) emissions (microscopic pictures of P and H band emissions are depicted in the Supplemental Material [36]).

The temperature-dependent energy shift of the $\Gamma_1^{\mathrm{L}}$ spontaneous emission peak was obtained experimentally (Fig. 2). The $\Gamma_1^{\mathrm{T}}$ state has an energy 9.3 meV lower than that of the $\Gamma_1^{\mathrm{L}}$ state [35]. The temperature dependence of the $\Gamma_1^{\mathrm{L,T}}$-$m$LO spontaneous emission peak energies ($E_{\Gamma_1^{\mathrm{L,T}}}^{m\mathrm{LO}}$) can be estimated by the following equation [13]:

$$E_{\Gamma_1^{\mathrm{L,T}}}^{m\mathrm{LO}} = E_{\Gamma_1^{\mathrm{L,T}}} - m\hbar\omega_{\mathrm{LO}} + \left(\frac{5}{2} - m\right)k_{\mathrm{B}}T \quad (m = 1, 2), \quad (1)$$

where $E_{\Gamma_1^{\mathrm{L,T}}}$, $m$, $\hbar\omega_{\mathrm{LO}}$, $k_{\mathrm{B}}$, and $T$ are the $\Gamma_1^{\mathrm{L}}$ or $\Gamma_1^{\mathrm{T}}$ emission peak energy, number of phonons involved, LO phonon energy, Boltzmann constant, and temperature, respectively. Haug has reported that the stimulated emission peak energy (gain spectrum) is approximately the same as the spontaneous emission peak energy (spectrum) at low temperatures [46]. In our experiments, the detection geometry of stimulated emission is $k \perp c$, where $k$ and $c$ are the Poynting vector of luminescence signals and the $c$ axis of wurtzite crystals, respectively. Consequently, we consider the $\Gamma_1^{\mathrm{T}}$-$m$LO transitions (not $\Gamma_1^{\mathrm{L}}$-$m$LO transitions) as free-exciton LO-phonon replica emissions (Fig. 3).

The spontaneous emission peak energy of the P band, $E(\mathrm{P})$, can be described as [13]

$$E(\mathrm{P}) = E_{\mathrm{exciton}}^{\mathrm{P}} - E_{\mathrm{exc}}^{\mathrm{bind}}(1 - 1/n^2), \quad n = 2, 3, \ldots, \infty, \quad (2)$$

where $E_{\mathrm{exciton}}^{\mathrm{P}}$ and $E_{\mathrm{exc}}^{\mathrm{bind}}$ are the energy and binding energy of an excitonic state involving the P band emission, respectively. A kinetic term is not included in Eq. (2) [13]. Previous studies have shown that the spontaneous and stimulated emission spectra have a low-energy tail [47,48]. The most likely candidate for the excitonic state is the energetically lowest exciton–that is, the $\Gamma_5$ (dipole-allowed) and $\Gamma_2$ (spin-forbidden) states for AlN. The two excitonic states have approximately the same energy [31]. The reported exciton binding energy is 67.3 meV [20]. In the present study, we treat the $\mathrm{P}^{\infty}$ ($n = \infty$) transition as the P band emissions (Fig. 3).

The spontaneous emission peak energy of the H band $E(\mathrm{H})$ can be expressed as [49]

$$E(\mathrm{H}) = E_{\mathrm{exciton}}^{\mathrm{H}} - \gamma k_{\mathrm{B}}T, \quad (3)$$

where $E_{\mathrm{exciton}}^{\mathrm{H}}$ is the energy of an excitonic state involving the H band emission. Previous studies have found that the spontaneous and stimulated emission (gain) spectra have a low-energy tail [49,50]. We assign the $\Gamma_2$ and $\Gamma_5$ excitons to the excitonic state of $E_{\mathrm{exciton}}^{\mathrm{H}}$ for AlN. Parameter $\gamma$ is a constant related to the translational exciton mass $M$ and the electron effective mass $m_e$. For example, Klingshirn proposed $\gamma = 3/2(M/m_e - 1 + 1.7\sqrt{M/m_e})$ [13], whereas Yu *et al.* proposed $\gamma = M/(2m_e)$ [51]. A more sophisticated theory agrees well with the former model in the case of ZnO [49]. Parameter $M$ is defined by $M = m_e + m_h$, where $m_h$ is the hole effective mass (crystal-field split-off hole for AlN); $m_{e,h}$ is the averaged effective mass and is defined as $1/m_e = (2/m_{\perp,e} + 1/m_{\parallel,e})/3$ and $1/m_h = (2/m_{\perp,h} + 1/m_{\parallel,h})/3$; $m_{\parallel,e}$ and $m_{\parallel,h}$ are the effective masses of an electron and a hole parallel to the $c$ axis, respectively; $m_{\perp,e}$ and $m_{\perp,h}$ are the effective masses of an electron and a hole perpendicular to the $c$ axis, respectively. For the effective mass values of AlN, we used $m_{\parallel,e} = 0.32m_0$, $m_{\perp,e} = 0.30m_0$, $m_{\parallel,h} = 0.26m_0$, and $m_{\perp,h} = 3.89m_0$, as deduced from Ref. [52], where $m_0$ is the electron mass in vacuum.

To get an insight into the spontaneous and stimulated emission peaks of an EHP emission, we estimated the band gap renormalization energy $\Delta E_g$ [53]. A dimensionless parameter $r_s$ is defined by $[(4\pi a_{\rm B}^3/3)n_{eh}]^{-1/3}$, where $a_{\rm B}$ and $n_{eh}$ are the exciton Bohr radius and electron–hole pair density, respectively. The exciton Bohr radius of AlN was derived as 1.25 nm from the exciton binding energy [20] and dielectric constants [54]. At the excitation power density of 7 MW/cm$^2$ (around threshold at 293 K), the estimated electron–hole pair density is $1.5 \times 10^{19}$ cm$^{-3}$. Here, we assume that AlN has a carrier lifetime of 10 ps [55], an absorption coefficient at 193 nm of $2.9 \times 10^5$ cm$^{-1}$ [54], and a refractive index at 193 nm of 2.91 [54]. The estimated $r_s$ is 2.0. Using the $r_s$ and $\Delta E_g$ universal relation [53], we estimated $\Delta E_g$ to be approximately 210 meV. This value is the maximum $\Delta E_g$ because we herein assume that the electron–hole pair density is equal to the photogenerated particle density (i.e., we neglect the exciton concentration in this estimation.). Notably, other theories give smaller $\Delta E_g$ values [44,56]. The spontaneous and stimulated emission peaks of an EHP emission must have energies greater than $E_g - \Delta E_g$, where $E_g$ is the band gap (not the excitonic energy) [44].

Figure 5 summarizes spontaneous and stimulated emission peak energies of AlN. From 11 K to 50 K, we assign the first- and second-threshold–stimulated emission mechanisms to the $P^\infty$ and $\Gamma_1^{\rm T}$-1LO band emissions, respectively. The calculated spontaneous emission peak energies are in excellent agreement with the experimental stimulated emission peak energies. Notably, the energy position of the $P^\infty$ band (5.960 eV at 11 K) cannot be explained by the exciton–exciton scattering process of the $\Gamma_1^{\rm L,T}$ states [according to Eq. (2), the $P^\infty$ band of the $\Gamma_1^{\rm L}$ and $\Gamma_1^{\rm T}$ states has a photon energy of 5.973 eV and 5.965 eV at 11 K, respectively]. Because of the discrepancy in the photon energy and spectral shape, we also rule out the possibility that the first-threshold stimulated emission arises from the TES emission: the TES emission has a peak energy of 5.964 eV and a FWHM of 4.5 meV at 11 K (Fig. 2), whereas the peak at 5.960 eV has a FWHM of 10.7 meV [at the lowest excitation-power density in Fig. 3(a)]. In the range from 50 K to 125 K, the stimulated emission mechanism is attributed to the $\Gamma_1^{\rm T}$-1LO band because of the peak energy and spectral shape (high-energy tail). The slight redshift of the stimulated emission from the spontaneous emission at 125 K is ascribed to high carrier temperature and/or reabsorption effects, as observed for other materials [11–13].

To discuss the stimulated emission mechanism that occurs at temperatures above 125 K, we first eliminate the possibility that the stimulated emission originates from the EHP band. The reduced band gap $E_g' = E_g - \Delta E_g$ at RT was estimated using a relation in Ref. [53] and is depicted in Fig. 5. The experimentally observed stimulated emission peak is located at an energy lower than $E_g'$, suggesting that the stimulated emission is not attributable to the EHP band at RT. Feneberg *et al.* observed a RT EHP spontaneous emission for AlN bulk crystals at 5.85 eV under excitation conditions ranging from 5 MW/cm$^2$ to 24 MW/cm$^2$ [57]; their experimental results are consistent with our discussion. Because the EHP emission emerges as the temperature increases [44], the EHP band is not the origin of the stimulated emission at all of the experimental temperatures.

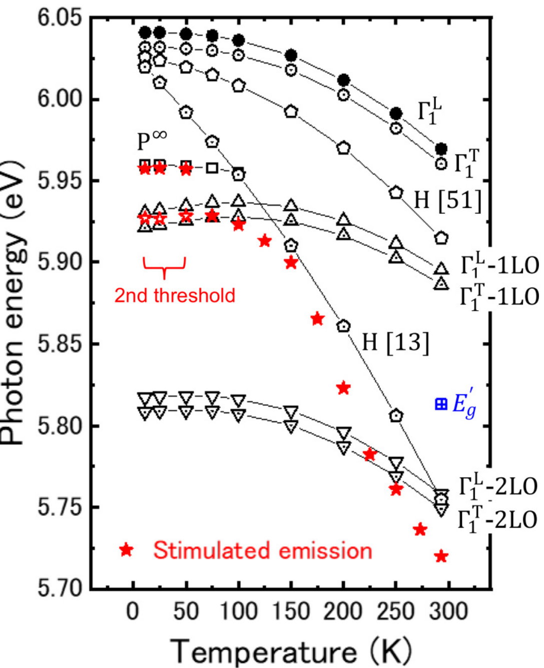


FIG. 5. Temperature dependence of spontaneous ($\Gamma_1^{\rm L,T}$, $\Gamma_1^{\rm L,T}$-$m$LO, $P^\infty$, and H band) and stimulated emission peak energies for a HVPE-grown AlN substrate. The temperature dependence of the $\Gamma_1^{\rm L}$ spontaneous emission peak (solid black circles) and stimulated emission peaks (solid and open red stars) are experimentally obtained. The term "2nd threshold" in the figure represents the second stimulated emission by the $\Gamma_1^{\rm T}$-1LO band shown in Figs. 3(a) and 3(b). The energy of the $\Gamma_1^{\rm T}$ is set 9.3 meV lower than that of the $\Gamma_1^{\rm L}$ state [35]. The peak energies of spontaneous emission lines (open black symbols) except the $\Gamma_1^{\rm L}$ emission peak are theoretically estimated by the method described in the main text. Two theoretical models (H [13] and H [51] in the figure) are used for the H band calculation. $E_g'$ is the reduced band gap defined by $E_g' = E_g - \Delta E_g$. The spontaneous and stimulated emission peak energies of an EHP emission must be greater than $E_g'$.

Next, we shift the discussion to the H band. Using two models [13,51], we calculated the temperature dependence of the H band according to Eq. (3); the results are depicted in Fig. 5. The calculated result obtained using the $\gamma$ value reported in Ref. [13] agrees well with the experimental stimulated emission peak energies. Because a rigorous theory [49] supports the $\gamma$ of Ref. [13] in ZnO (a material similar to AlN), we speculate that the agreement between the theory and experiment is not accidental but critical. The theory proposed in Ref. [49] can also explain the excitation-power–induced redshift in Fig. 3. Therefore, we conclude that the H band is one origin of the stimulated emission at temperatures from 125 K to 250 K (at 125 K, both the $\Gamma_1^{\rm T}$-1LO and H bands should contribute to the stimulated emission).

Finally, we consider the stimulated emission mechanism from 250 K to 293 K. Figure 6 shows the temperature dependence of the threshold power density of the HVPE-grown AlN substrate. Figures 5 and 6 suggest that the stimulated emission mechanism might change at 250 K. According to the spectral positions, in addition to the H band, the $\Gamma_1^{\rm T}$-2LO band should contribute to the stimulated emission. Previous works have

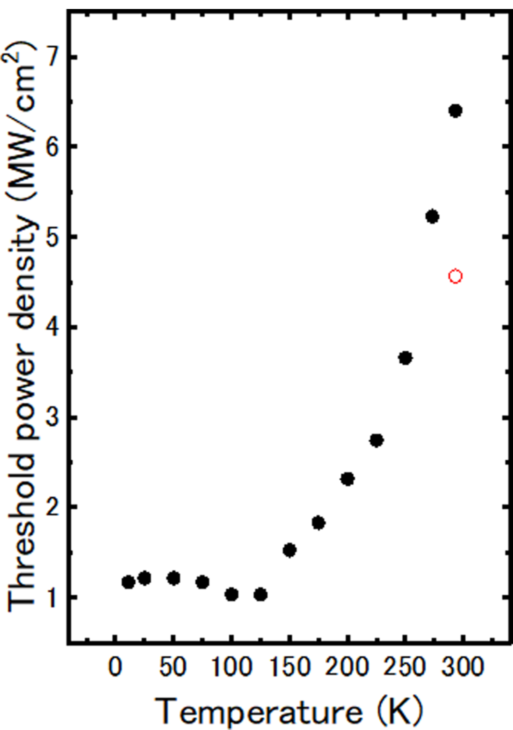


FIG. 6. Temperature dependence of the threshold power density for a HVPE-grown AlN substrate. The threshold power density differs depending on the irradiated position of the sample, possibly due to the spatial inhomogeneities of the cleaved edge surfaces and/or inner crystalline qualities. Most positions of the sample had a threshold power density plotted by solid black circles. The lowest threshold power density we found is 4.6 $\mathrm{MW/cm^2}$ at 293 K (red open circle). Although the spatial variation of the threshold power density below 293 K is not quantified, it should be almost the same or less than the spatial variation at 293 K (nonradiative recombinations at defects are generally suppressed as temperature decreases).

theoretically [46] and experimentally [13] discussed the emergence of the EX-2LO transition at high temperatures in other materials. Because the appearance of the H band indicates the (at least partial) dissociation of excitons, the stimulated emission mechanism should not be assigned solely to the $\Gamma_1^\mathrm{T}$-2LO band. For the investigated experimental temperature ranges, the redshift of the experimental stimulated emission peaks compared with the estimated spontaneous emission peaks is attributable to excitation-induced damping, polaron mass correction, higher carrier temperature, and reabsorption effects, similar to the redshift observed for other materials [11–13,23,24,44]. We conclude that the stimulated emission mechanism of AlN at temperatures above 125 K is not purely excitonic and also does not originate from degenerated EHP emissions.

Table I summarizes stimulated emission mechanisms in select semiconductors. Similar to other materials, AlN exhibits a universal temperature-induced crossover of the stimulated emission mechanism, where the purely excitonic emission (EX-1LO band) at low temperatures changes to the carrier-involved emission (H band) at high temperatures. However, contrary to our observation, a previous study has reported that, for CdS at low temperatures, the P band overtook the EX-1LO band because of the low gain generation of the latter process [59]. This behavior is reasonably explained by the EX-1LO band emission being a linear recombination process and the P band emission being a quadratic recombination process [14,15,44]. Therefore, we observed an unusual excitation-power–induced crossover for AlN. We can explain this crossover behavior of AlN in terms of its peculiar excitonic structure. As noted, the most likely candidates for the initial state of the P band emission are the $\Gamma_2$ and $\Gamma_5$ states because they are the energetically lowest excitonic states as a consequence of the negative crystal-field splitting and positive electron–hole exchange interaction energies in AlN [31,43]. On the other hand, we experimentally confirmed that the $\mathrm{P}^\infty$ and $\Gamma_1^\mathrm{T}$-1LO band emissions after the threshold exhibited an optical polarization of $E \parallel c$ (see Fig. S5 in the Supplemental Material [36]), indicating that the interstitial state of the P band emission is the $\Gamma_1$ state. The difference in the excitonic state between the initial and interstitial states (this statement does not hold for other materials) should lead to the observed low transition probability of the P band emission in AlN.

TABLE I. Stimulated emission mechanism in select semiconductors.

| Material | Stimulated emission mechanism |
|---|---|
| ZnO [13] | P band < 70 K, H band > 70 K |
| ZnO [13] | EX-1LO band ⩽ 115 K, EX-2LO band ⩾ 105 K |
| ZnO [19] | P band ⩽ 150 K, H band ⩾ 150 K |
| GaN [22] | EHP band at 8 K |
| GaN [23] | P band < 150 K, EHP band ⩾ 150 K |
| GaN [24] | P band < 145 K, EHP band ⩾ 145 K |
| GaN [25] | P or H band < 440 K (EHP band ⩾ 8 K) |
| GaN [26] | H band from 120 K to RT |
| CdS [58] | EX-1LO ⩽ 120 K, H band > 120 K |
| AlN (this work) | P band ⩽ 50 K, EX-1LO band ⩽ 125 K, H band ⩾ 125 K (EX-2LO band superimposes ⩾ 250 K) |

We here consider the thermodynamic equilibrium between excitons and free electron–hole pairs in AlN. The total particle density $n_\mathrm{total}$ is defined by $n_\mathrm{total} = n_{eh} + n_\mathrm{exc}$, where $n_\mathrm{exc}$ is the exciton density. The fraction of free electron–hole pairs with respect to the total particle density, $x = n_{eh}/n_\mathrm{total}$, can be expressed by the Saha equation [60,61]:

$$\frac{x^2}{1-x} = \frac{1}{n_\mathrm{total}}\left(\frac{2\pi \mu k_\mathrm{B} T}{h^2}\right)^{3/2} \exp\left(-\frac{E_\mathrm{exc}^\mathrm{bind}}{k_\mathrm{B} T}\right), \tag{4}$$

where $\mu$ and $h$ are the reduced exciton mass ($1/\mu = 1/m_e + 1/m_h$) and Planck's constant, respectively. Figure 7(a) shows a plot of the calculated results obtained using Eq. (4) under several fixed $E_\mathrm{exc}^\mathrm{bind}$ (broken lines). We then consider the free electron–hole pair density dependence of the exciton binding energy. Using the $r_s$ and $\Delta E_g$ relation in Ref. [53] and assuming that the absolute exciton energy $E_\mathrm{exc}$ is independent of $n_{eh}$ [44], we derive the relation between $r_s$ and $E_\mathrm{exc}^\mathrm{bind} = (E_g - \Delta E_g) - E_\mathrm{exc}$ as shown in Fig. 7(b). Note that the negative $E_\mathrm{exc}^\mathrm{bind}$ indicates that excitons are not energetically favorable. The final results are plotted as red circles in Fig. 7(a). Here, it must be recalled that the transition probability of the H

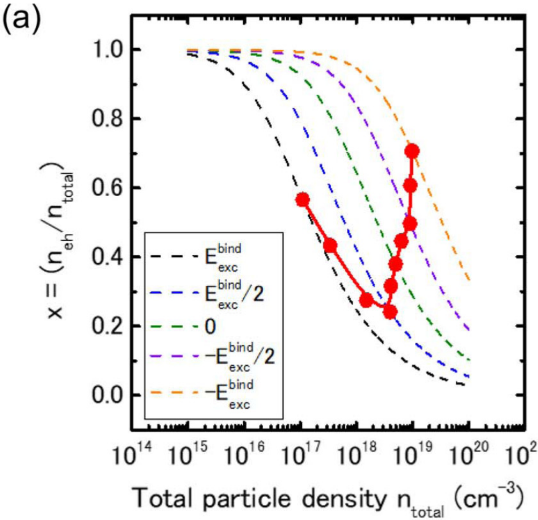


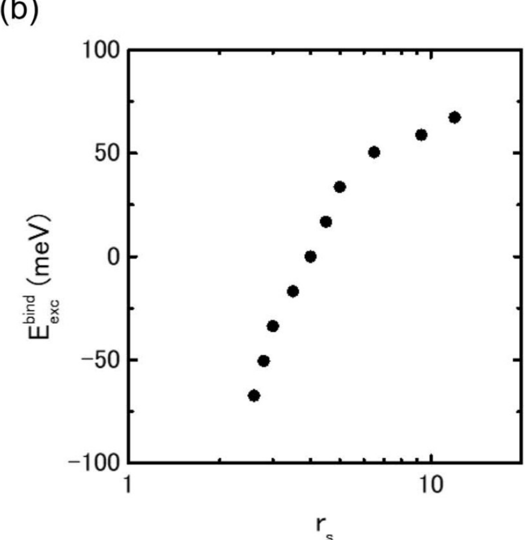


FIG. 7. (a) Free electron–hole pair density fraction, $x = n_{eh}/n_{\text{total}}$, as a function of the total particle density, $n_{\text{total}}$, of AlN at 293 K. $E_{\text{exc}}^{\text{bind}}$ is 67.3 meV. Red circles are the solutions that consider the free electron–hole pair density dependence of the exciton binding energy. The red line is generated by a B-spline interpolation. (b) $r_s$ and $E_{\text{exc}}^{\text{bind}}$ relation for AlN. $r_s$ is defined as $[(4\pi a_{\text{B}}^3/3)n_{eh}]^{-1/3}$, where $a_{\text{B}}$ and $n_{eh}$ are the exciton Bohr radius and free electron–hole pair density, respectively. $E_{\text{exc}}^{\text{bind}}$ is defined as $(E_g - \Delta E_g) - E_{\text{exc}}$, where the absolute exciton energy $E_{\text{exc}}$ is assumed to be independent of $n_{eh}$ [44].

band is maximal when the exciton and free electron–hole pair densities are the same ($x = 0.5$) [49,50]. Figure 7(a) suggests that the H band emission is an efficient process near the threshold ($n_{\text{total}} \sim 10^{19}$ cm$^{-3}$) at RT, which is consistent with our assignment of the stimulated emission in AlN. Toward practical applications, this consideration should suggest the importance of exciton-binding-energy engineering to realize continuous-wave and/or low-threshold AlGaN-based LDs. A simple approach should be to reduce the operating temperatures, as indicated in Fig. 6 for AlN and in Ref. [23] for GaN. The optimum temperature should be approximately 100 K. Note that polarization-doped [62] AlGaN light-emitting devices are electrically active even at low temperatures [63].

We revealed that the shortest spontaneous and stimulated emission wavelengths of an unstrained AlGaN-alloy system (AlGaN-based DUV light-emitting devices are reviewed elsewhere [2,3]) are not the same wavelengths but ∼208 nm (the 5.969 eV peak in Fig. 2) and ∼217 nm [the 5.720 eV peak in Fig. 3(i)], respectively, at RT. The shortest stimulated emission wavelength is almost the same as the stimulated emission wavelength (215 nm) of hexagonal boron nitride [64], which is contrary to the case for the spontaneous emission wavelengths. Shorter stimulated emission wavelengths are desirable for enhancing the spatial resolution in lithography [65] and microspectroscopy [66].

For the sake of completeness, we here estimate the transparent electron–hole pair density in AlN (the method is described in the Supplemental Material [36]). The effective density of states at the conduction $N_c$ and valence $N_v$ band edges are given by $N_c = 2[(m_{\parallel,e}m_{\perp,e}^2)^{1/3}k_BT/(2\pi\hbar^2)]^{3/2}$ and $N_v = 2[(m_{\parallel,h}m_{\perp,h}^2)^{1/3}k_BT/(2\pi\hbar^2)]^{3/2}$, respectively. At 293 K, the estimated $N_c$ and $N_v$ are $4.1 \times 10^{18}$ cm$^{-3}$ and $4.8 \times 10^{19}$ cm$^{-3}$, respectively. The transparent electron–hole pair density is consequently derived as $9.3 \times 10^{18}$ cm$^{-3}$, which is similar to the free electron–hole pair density at around RT threshold (7 MW/cm$^2$). In addition, varying the irradiated position of the sample yielded a lower threshold power density of 4.6 MW/cm$^2$ at 293 K (Fig. 6). In this case, the free electron–hole pair density is lower than the transparent density at the threshold. When a finite loss is also considered, degenerated EHP is not an origin of stimulated emission in AlN, as previously discussed.

## V. CONCLUSIONS

In conclusion, HVPE-grown AlN substrates were characterized by photoluminescence and stimulated emission spectroscopies. We observed the stimulated emission from cryogenic to room temperatures. The stimulated emission mechanism was assigned on the basis of the spontaneous emission spectra and existing theories. Similar to other materials, AlN exhibited a temperature-induced crossover in which the purely excitonic stimulated emission mechanism changed to a carrier-involved one. However, we observed a unique excitation-power–induced crossover in which a phonon-mediated stimulated emission mechanism overtook an exciton–exciton scattering mechanism, which we attributed to the peculiar excitonic structure (negative crystal-field splitting and positive electron–hole exchange interaction energies) of AlN.

*Note added in proof.* Recently, a study demonstrated continuous-wave lasing of a 274.8 nm AlGaN-based LD [67]. The introduction in this manuscript is consequently not up-to-date, but we believe investigating the gain generation mechanism of AlN-related materials is still essential both for scientific and engineering side.

## ACKNOWLEDGMENTS

This work was partly supported by JSPS KAKENHI Grants No. JP19H02615 and No. JP20H05622.

[1] Y. Taniyasu, M. Kasu, and T. Makimoto, Nature (London) **441**, 325 (2006).
[2] M. Kneissl, T. Seong, J. Han, and H. Amano, Nat. Photon. **13**, 233 (2019).
[3] H. Amano, R. Collazo, C. D. Santi, S. Einfeldt, M. Funato, J. Glaab, S. Hagedorn, A. Hirano, H. Hirayama, R. Ishii, Y. Kashima, Y. Kawakami, R. Kirste, M. Kneissl, R. Martin, F. Mehnke, M. Meneghini, A. Ougazzaden, P. J. Parbrook, S. Rajan *et al.*, J. Phys. D: Appl. Phys. **53**, 503001 (2020).
[4] Z. Zhang, M. Kushimoto, T. Sakai, N. Sugiyama, L. J. Schowalter, C. Sasaoka, and H. Amano, Appl. Phys. Express **12**, 124003 (2019).
[5] K. Sato, S. Yasue, K. Yamada, S. Tanaka, T. Omori, S. Ishizuka, S. Teramura, Y. Ogino, S. Iwayama, H. Miyake, M. Iwaya, T. Takeuchi, S. Kamiyama, and I. Akasaki, Appl. Phys. Express **13**, 031004 (2020).
[6] M. Martens, C. Kuhn, T. Simoneit, S. Hagedorn, A. Knauer, T. Wernicke, M. Weyers, and M. Kneissl, Appl. Phys. Lett. **110**, 081103 (2017).
[7] R. Kirste, Q. Guo, J. H. Dycus, A. Franke, S. Mita, B. Sarkar, P. Reddy, J. M. LeBeau, R. Collazo, and Z. Sitar, Appl. Phys. Express **11**, 082101 (2018).
[8] Q. Guo, R. Kirste, S. Mita, J. Tweedie, P. Reddy, B. Moody, Y. Guan, S. Washiyama, A. Klump, Z. Sitar, and R. Collazo, J. Appl. Phys. **126**, 223101 (2019).
[9] Z. Zhang, M. Kushimoto, T. Sakai, N. Sugiyama, L. J. Schowalter, C. Sasaoka, and H. Amano, Jpn. J. Appl. Phys. **59**, 094001 (2020).
[10] S. Tanaka, Y. Ogino, K. Yamada, T. Omori, R. Ogura, S. Teramura, M. Shimokawa, S. Ishizuka, A. Yabutani, S. Iwayama, K. Sato, H. Miyake, M. Iwaya, T. Takeuchi, S. Kamiyama, and I. Akasaki, Appl. Phys. Lett. **118**, 163504 (2021).
[11] R. F. Leheny, K. L. Shaklee, E. P. Ippen, R. E. Nahory, and J. L. Shay, Appl. Phys. Lett. **17**, 494 (1970).
[12] J. M. Hvam, Phys. Rev. B **4**, 4459 (1971).
[13] C. Klingshirn, Phys. Status Solidi B **71**, 547 (1975).
[14] S. W. Koch, H. Haug, G. Schmieder, W. Bohnert, and C. Klingshirn, Phys. Status Solidi B **89**, 431 (1978).
[15] C. Klingshirn and H. Haug, Phys. Rep. **70**, 315 (1981).
[16] J. Ding, H. Jeon, T. Ishihara, M. Hagerott, A. V. Nurmikko, H. Luo, N. Samarth, and J. Furdyna, Phys. Rev. Lett. **69**, 1707 (1992).
[17] H. D. Sun, T. Makino, N. T. Tuan, Y. Segawa, Z. K. Tang, G. K. L. Wong, M. Kawasaki, A. Ohtomo, K. Tamura, and H. Koinuma, Appl. Phys. Lett. **77**, 4250 (2000).
[18] C. Klingshirn, R. Hauschild, J. Fallert, and H. Kalt, Phys. Rev. B **75**, 115203 (2007).
[19] R. Matsuzaki, H. Soma, K. Fukuoka, K. Kodama, A. Asahara, T. Suemoto, Y. Adachi, and T. Uchino, Phys. Rev. B **96**, 125306 (2017).
[20] R. Ishii, M. Funato, and Y. Kawakami, Jpn. J. Appl. Phys. **53**, 091001 (2014).
[21] H. Murotani, R. Tanabe, K. Hisanaga, A. Hamada, K. Beppu, N. Maeda, M. A. Khan, M. Jo, H. Hirayama, and Y. Yamada, Appl. Phys. Lett. **117**, 162106 (2020).
[22] S. Hess, R. A. Taylor, J. F. Ryan, B. Beaumont, and P. Gibart, Appl. Phys. Lett. **73**, 199 (1998).
[23] S. Bidnyk, T. J. Schmidt, B. D. Little, and J. J. Song, Appl. Phys. Lett. **74**, 1 (1999).
[24] W. D. Herzog, G. E. Bunea, M. S. Ünlü, B. B. Goldberg, and R. J. Molnar, Appl. Phys. Lett. **77**, 4145 (2000).
[25] K. Kazlauskas, G. Tamulaitis, A. Žukauskas, T. Suski, P. Perlin, M. Leszczynski, P. Prystawko, and I. Grzegory, Phys. Rev. B **69**, 245316 (2004).
[26] M. Nakayama, H. Tanaka, M. Ando, and T. Uemura, Appl. Phys. Lett. **89**, 031909 (2006).
[27] M. Shatalov, M. Gaevski, V. Adivarahan, and A. Khan, Jpn. J. Appl. Phys. **45**, L1286 (2006).
[28] Y. Kumagai, Y. Kubota, T. Nagashima, T. Kinoshita, R. Dalmau, R. Schlesser, B. Moody, J. Xie, H. Murakami, A. Koukitu, and Z. Sitar, Appl. Phys. Express **5**, 055504 (2012).
[29] T. Nagashima, R. Ishikawa, T. Hitomi, R. Yamamoto, J. Kotani, and Y. Kumagai, J. Cryst. Growth **540**, 125644 (2020).
[30] M. Funato, K. Matsuda, R. G. Banal, R. Ishii, and Y. Kawakami, Appl. Phys. Express **5**, 082001 (2012).
[31] R. Ishii, M. Funato, and Y. Kawakami, Phys. Rev. B **87**, 161204(R) (2013).
[32] M. Kaneko, H. Okumura, R. Ishii, M. Funato, Y. Kawakami, T. Kimoto, and J. Suda, Appl. Phys. Express **6**, 062604 (2013).
[33] S. F. Chichibu, K. Hazu, Y. Ishikawa, M. Tashiro, T. Ohtomo, K. Furusawa, A. Uedono, S. Mita, J. Xie, R. Collazo, and Z. Sitar, Appl. Phys. Lett. **103**, 142103 (2013).
[34] S. F. Chichibu, K. Kojima, K. Hazu, Y. Ishikawa, K. Furusawa, S. Mita, R. Collazo, Z. Sitar, and A. Uedono, Appl. Phys. Lett. **115**, 151903 (2019).
[35] R. Ishii, M. Funato, and Y. Kawakami, Phys. Rev. B **102**, 155202 (2020).
[36] See Supplemental Material at http://link.aps.org/supplemental/10.1103/PhysRevB.105.205206 for microscopic mechanism of optical transitions, optical polarization properties of excitonic recombination processes in AlN, excitation-power-dependence analysis of stimulated emission spectra of AlN, and a transparent electron–hole density estimation method.
[37] B. Neuschl, K. Thonke, M. Feneberg, S. Mita, J. Xie, R. Dalmau, R. Collazo, and Z. Sitar, Phys. Status Solidi B **249**, 511 (2012).
[38] R. Ishii, A. Yoshikawa, H. Kobayashi, M. Funato, and Y. Kawakami, Jpn. J. Appl. Phys. **60**, 080901 (2021).
[39] B. Neuschl, K. Thonke, M. Feneberg, R. Goldhahn, T. Wunderer, Z. Yang, N. M. Johnson, J. Xie, S. Mita, A. Rice, R. Collazo, and Z. Sitar, Appl. Phys. Lett. **103**, 122105 (2013).
[40] J. M. Hayes, M. Kuball, Y. Shi, and J. H. Edger, Jpn. J. Appl. Phys. **39**, L710 (2000).
[41] C. Reich, M. Feneberg, V. Kueller, A. Knauer, T. Wernicke, J. Schlegel, M. Frentrup, R. Goldhahn, M. Weyers, and M. Kneissl, Appl. Phys. Lett. **103**, 212108 (2013).
[42] R. Ishii, A. Kaneta, M. Funato, Y. Kawakami, and A. A. Yamaguchi, Phys. Rev. B **81**, 155202 (2010).
[43] R. Ishii, A. Kaneta, M. Funato, and Y. Kawakami, Phys. Rev. B **87**, 235201 (2013).
[44] C. Klingshirn, *Semiconductor Optics*, 2nd ed. (Springer, Berlin, 2005).
[45] B. Segall and G. D. Mahan, Phys. Rev. **171**, 935 (1968).
[46] H. Haug, J. Appl. Phys. **39**, 4687 (1968).
[47] I. Pelant and J. Valenta, *Luminescence Spectroscopy of Semiconductors* (Oxford University Press, New York, 2012).
[48] T. Moriya and T. Kushida, J. Phys. Soc. Jpn. **40**, 1676 (1976).

[49] B. Hönerlage, C. Klingshirn, and J. B. Grun, Phys. Status Solidi B **78**, 599 (1976).
[50] H. Haug and S. Koch, Phys. Status Solidi B **82**, 531 (1977).
[51] C. I. Yu, T. Goto, and M. Ueta, J. Phys. Soc. Jpn. **34**, 693 (1973).
[52] I. Vurgaftman and J. R. Meyer, J. Appl. Phys. **94**, 3675 (2003).
[53] T. J. Inagaki and M. Aihara, Phys. Rev. B **65**, 205204 (2002).
[54] M. Feneberg, M. F. Romero, M. Röppischer, C. Cobet, N. Esser, B. Neuschl, K. Thonke, M. Bickermann, and R. Goldhahn, Phys. Rev. B **87**, 235209 (2013).
[55] T. Onuma, K. Hazu, A. Uedono, T. Sota, and S. F. Chichibu, Appl. Phys. Lett. **96**, 061906 (2010).
[56] P. Vashishta and R. K. Kalia, Phys. Rev. B **25**, 6492 (1982).
[57] M. Feneberg, R. A. R. Leute, B. Neuschl, K. Thonke, and M. Bickermann, Phys. Rev. B **82**, 075208 (2010).
[58] W. Wünstel and C. Klingshirn, Opt. Commun. **32**, 269 (1980).
[59] C. B. Guillaume, J. M. Debever, and F. Salban, Phys. Rev. **177**, 567 (1969).
[60] R. Cingolani, L. Calcagnile, G. Colí, R. Rinaldi, M. Lomoscolo, M. Didio, A. Franciosi, L. Vanzetti, G. C. LaRocca, and D. Campi, J. Opt. Soc. Am. B **13**, 1268 (1996).
[61] V. D'lnnocenzo, G. Grancini, M. J. P. Alcocer, A. R. S. Kandada, S. D. Stranks, M. M. Lee, G. Lanzani, H. J. Snaith, and A. Petrozza, Nat. Commun. **5**, 3586 (2014).
[62] J. Simon, V. Protasenko, C. Lian, H. Xing, and D. Jena, Science **327**, 60 (2010).
[63] R. Ishii, A. Yoshikawa, K. Nagase, M. Funato, and Y. Kawakami, AIP Adv. **10**, 125014 (2020).
[64] K. Watanabe, T. Taniguchi, and H. Kanda, Nat. Mater. **3**, 404 (2004).
[65] T. Ito and S. Okazaki, Nature (London) **406**, 1027 (2000).
[66] R. Ishii, M. Funato, and Y. Kawakami, APL Photon. **4**, 070801 (2019).
[67] Z. Zhang, M. Kushimoto, A. Yoshikawa, K. Aoto, L. J. Schowalter, C. Sasaoka, and H. Amano, Appl. Phys. Express **15**, 041007 (2022).